SUPPLEMENTARY MATERIAL

DIVERSITY IN THE C3B CONTACT RESIDUES AND TERTIARY STRUCTURES OF THE STAPHYLOCOCCAL COMPLEMENT INHIBITOR (SCIN) PROTEIN FAMILY*.

Brandon L. Garcia[‡], Brady J. Summers[‡], Zhuoer Lin[§], Kasra X. Ramyar[‡], Daniel Ricklin[§], Divya V. Kamath[‡], Zheng-Qing Fu[**], John D. Lambris[§], and Brian V. Geisbrecht[‡,1]

From [‡]Division of Cell Biology and Biophysics, School of Biological Sciences, University of Missouri-Kansas City, Kansas City, Missouri 64110; [§]Department of Pathology and Laboratory Medicine, School of Medicine, University of Pennsylvania, Philadelphia, Pennsylvania, 19104;[**] Advanced Photon Source, Argonne National Laboratory, Argonne, Illinois, 60439

Running Head: Structural Characterization of *S. aureus* SCIN-B and SCIN-D.

Author to whom correspondence should be addressed: Brian V. Geisbrecht; E-mail GeisbrechtB@umkc.edu; School of Biological Sciences, University of Missouri-Kansas City, 5100 Rockhill Road, Kansas City, MO 64110; Tel. 816-235-2592, Fax. 816-235-1503.

SUPPLEMENTARY REFERENCES

S1. **Rocchia, W., Sridharan, S., Nicholls, A., Alexov, E., Chiabrera, A., and Honig, B. (2002) *J. Comput. Chem.* 23, 128-137**

S2. **Rocchia, W., Alexov, E., and Honig, B. (2001) *J. Phys. Chem. B* 105, 6507-6514**

S3. **Lawrence, M. C., and Colman, P. M. (1993) *J. Mol. Biol.* 234, 946-950**

SUPPLEMENTARY FIGURE LEGENDS

Fig. S1. SCIN sequence alignment. *A*, Sequence alignment was performed using ClustalW and mapped onto the secondary structure of SCIN-A and SCIN-D by ESPript (http://espript.ibcp.fr/ESPript/ESPript/). Secondary structure elements for SCIN-A were derived from the C3c/SCIN-A crystal structure (PDB #3OHX, chain M), while those for SCIN-D were derived from its full-length crystal structure (PDB #3T46). Residues that comprise the first (green stars) and second (blue arrowheads) C3c contact sites for SCIN-A are denoted, as are the C3c contact residues for SCIN-B$^{(18\text{-}85)}$ (red stars). For reference, the beginning of the SCIN-B$^{(18\text{-}85)}$ protein is denoted with an orange arrow. *B*, Identification of a protease-resistant fragment of SCIN-B by limited subtilisin digestion. A sample purified recombinant SCIN-B (1 μg/μl) was incubated with decreasing concentrations of subtilisin for 1 hr at 20 °C. The degradation products were separated by SDS-PAGE and visualized by staining with Coomassie brilliant blue.

Fig. S2. Representative model/map correlation in the refined C3c/SCIN-B$^{(18\text{-}85)}$ structure. Two copies of the C3c/SCIN$^{(18\text{-}85)}$ complex comprise the asymmetric unit of this primitive orthorhombic crystal system (Table 1). Refined electron density ($2F_o$-F_c contoured 1.5σ) is shown as a blue cage, while the protein model is drawn as either purple (C3c polypeptides) or green (SCIN-B$^{(18\text{-}85)}$) ribbon. *A*, C3c β-chain (domains MG1-MG6β). *B*, C3c α'-chain fragment 1 (domain MG7). *C*, C3c α'-chain fragment 2 (domains MG8, anchor, and C345C). *D*, SCIN-B$^{(18\text{-}85)}$. Domain boundaries were assigned according to Janssen et al. (30).

Fig. S3. SCIN-B$^{(18\text{-}85)}$ competes with SCIN-B for C3b binding whereas SCIN-D does not. Results of an AlphaScreen bead-based binding assay, where competition for binding between various proteins and full-length SCIN-B was assessed. SCIN-B$^{(18\text{-}85)}$ (green dashed line) competes specifically but with reduced affinity compared to full-length SCIN-B (green solid line). In order to investigate the potential impact of the SCIN-D helical distortion on C3b binding, a point mutation was made (SCIN-D$^{(8\text{-}83)}$-H48A) to eliminate the Thr^{26}-His^{48} interaction described in Results. However, both SCIN-D full-length and SCIN-D$^{(8\text{-}83)}$-H48A fail to bind C3b in this assay, even at high concentrations.

Fig. S4. SCIN-B competes with fH for binding to C3b. *A* and *B*, The C3b/C3c surface recognized by SCIN-B is practically indistinguishable from that of SCIN-A (Fig. 1d). It also overlaps with the first two domains of fH, as judged by structural superposition of C3c/SCIN-$B^{(18-85)}$ with that of C3b/fH(1-4) (7). In both panels, SCIN-$B^{(18-85)}$ and fH(1-4) are drawn as orange and dark green ribbons, respectively, while C3b appears as silver surface. The C3c/C3b contact residues held in common by SCIN-$B^{(18-85)}$ and fH(1-4) are colored in red. *C*, Based upon the significant overlap of their C3c/C3b contact residues, an AlphaAssay was used to assess the ability of SCIN-B to compete with full-length fH for C3b binding. Assay format was identical to that shown in Fig. S3, with the exception that fH was used as the unlabeled competitor instead of a SCIN protein. The C3b/fH interaction fits of an apparent K_D value of 24 nM; interestingly, this is about one-thousand fold higher affinity than that previously determined (12.7 μM; (7)) for the minimal decay-accelerating fragment of fH (i.e. fH(1-4)). Thus, it appears that SCIN-B also renders inhibited convertases resistant to decay acceleration (17).

Fig. S5. Cleavage of C3 by a fluid-phase AP Convertase. The AP C3 convertase (C3bBb) was assembled by fD-dependent proteolysis of pro-convertase (C3bB). *A*, Conversion to C3bBb was nearly complete after 5 min of incubation with fD, as judged by the loss of fB and generation a ~60 kDa species corresponding fragment Bb; the ~33 kDa band corresponding to fragment Ba stains poorly by Coomassie brilliant blue. Convertase-dependent cleavage of C3 (α and β chains) into C3b (α' and β chains) and C3a was followed over the course of 1 hr by removing 10% of the total reaction volume for analysis by SDS-PAGE. The reaction shown here is representative for the incubation of 300 nM final concentration of C3bBb with 2 μM C3 substrate. *B*, Normalized band intensities for both the α and α' chains were plotted versus time. The Michaelis-Menten law provides a reasonable, but not strictly accurate description of convertase digestion of C3 due to time-dependent decay of the C3bBb convertase enzyme.

Fig. S6. Crystal structures of SCIN-D derived molecules. Superimposition of refined coordinates for native SCIN-$D^{(8-83)}$ (PDB #3T47; violet), SCIN-$D^{(8-83)}$-MSE (PDB #3T48; light pink), and full-length SCIN-D (PDB #3T46) drawn in ribbon format. The N termini lie at the bottom of the page, while the C termini face the top. Whereas all of these molecules possess a nearly identical secondary structure, several additional C-terminal residues were observed in full-length SCIN-D and are found in a random coil. Additional N-terminal residues were not observed.

Fig. S7. Electrostatic potential at the surfaces of SCIN proteins. DelPhi (S1,S2) was used to calculate the electrostatic potential at the surface for each SCIN protein. The color scheme represents regions of negative (red) and positive (blue) charge density contoured at ± 5 e/*k*T, while each ribbon structure is depicted using a rainbow where the N terminus is blue and the C terminus is red. To generate this figure, all three structures were superimposed and rotated 120° to obtain equivalent surface views corresponding to projections that directly face each of the three α helices. *A*, SCIN-A (PDB #2QFF). *B*, SCIN-$B^{(18-85)}$ (PDB #3T49). *C*, SCIN-$D^{(8-83)}$ (PDB #3T47).

Supplementary Table 1. Buried Surface Area and Shape Complementarities of C3c/SCIN Complexes and Models.

Structure/Model[a]	BSA[b] C3c α' Frag. 1 (Å^2)	SC[c]	BSA C3c β (Å^2)	SC	BSA Total (Å^2)	BSA Weighted SC[d]
SCIN-A	627.1	0.67	133.5	0.52	760.6	0.64
SCIN-B$^{(18-85)}$	597.5	0.55	196.8	0.72	794.3	0.59
SCIN-D$^{(8-83)}$ (model)	509.7	0.34	166.2	0.25	675.9	0.32
SCIN-D$^{(8-83)}$ (rotamer)	495.3	0.31	149.2	0.48	644.5	0.35

[a]Model structures were constructed by superimposing unbound molecules onto the SCIN protein in the C3c/SCIN-B$^{(18-85)}$ co-crystal structure.
[b]Buried Surface Area (BSA) was calculated by the EBI-PISA server interface analysis (36).
[c]Surface complementarity indices (SC) were calculated by the CCP4 program SC (S3).
[d]BSA Weighted S.C. values were calculated as the surface area weighted average of the two complementarity indices. This normalizes the overall surface contribution to complex formation.

Garcia et al, Fig. S1

A

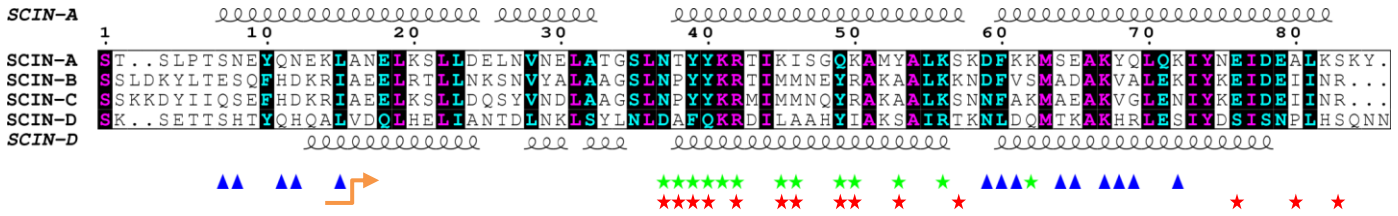

B

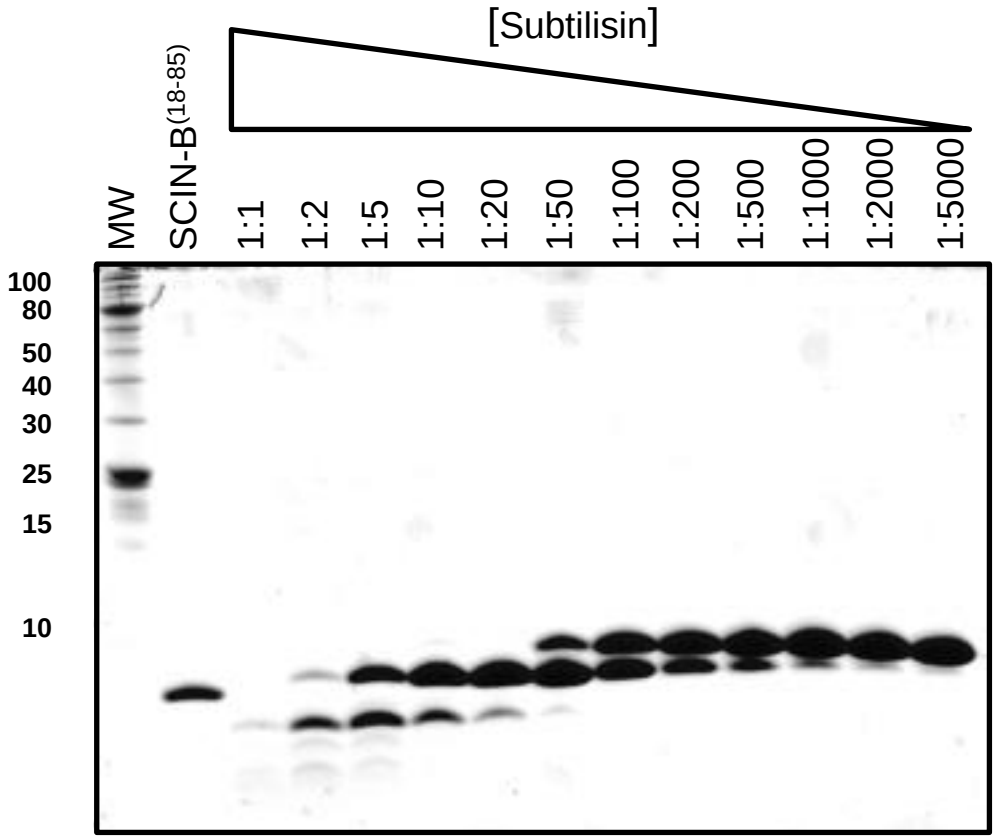

Garcia et al, Fig. S2

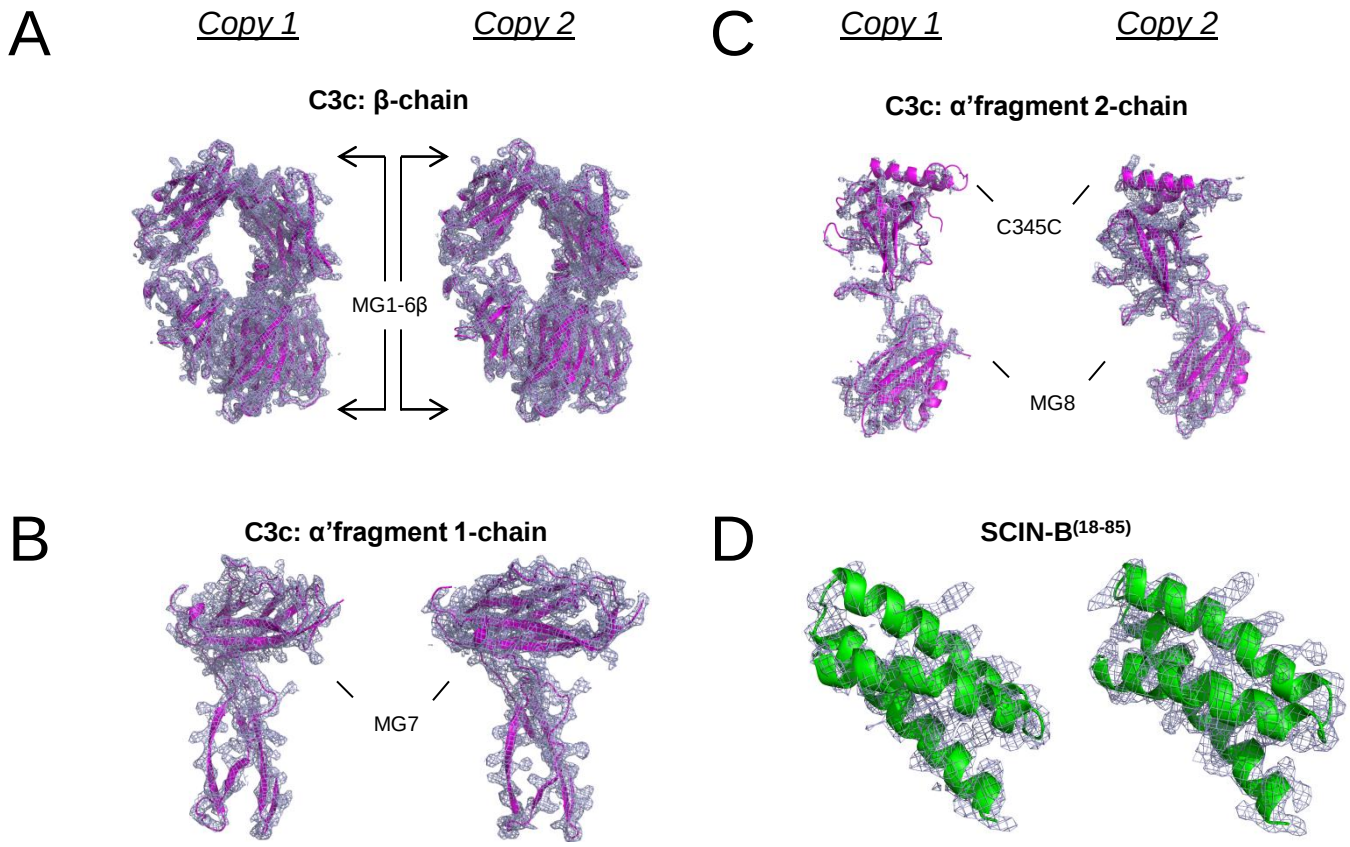

Garcia et al, Fig. S3

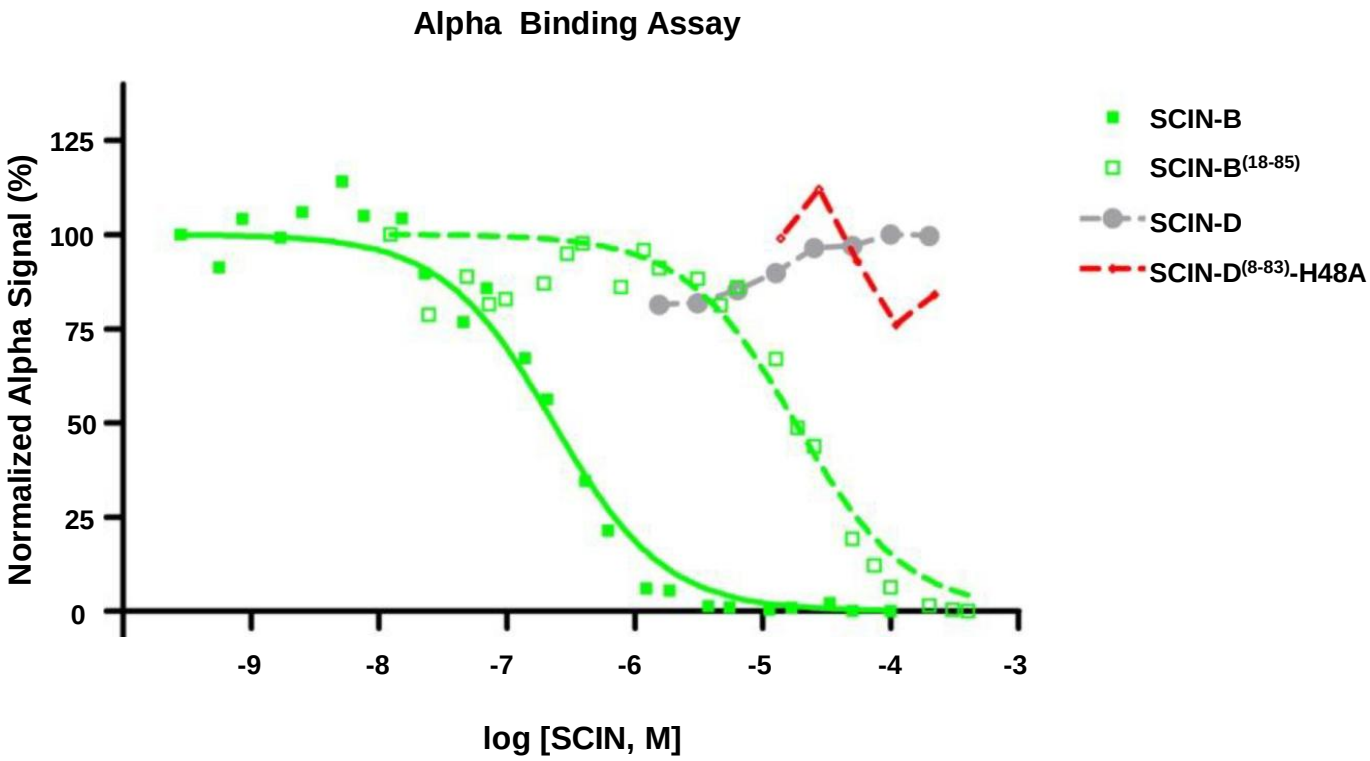

Garcia et al, Fig. S4

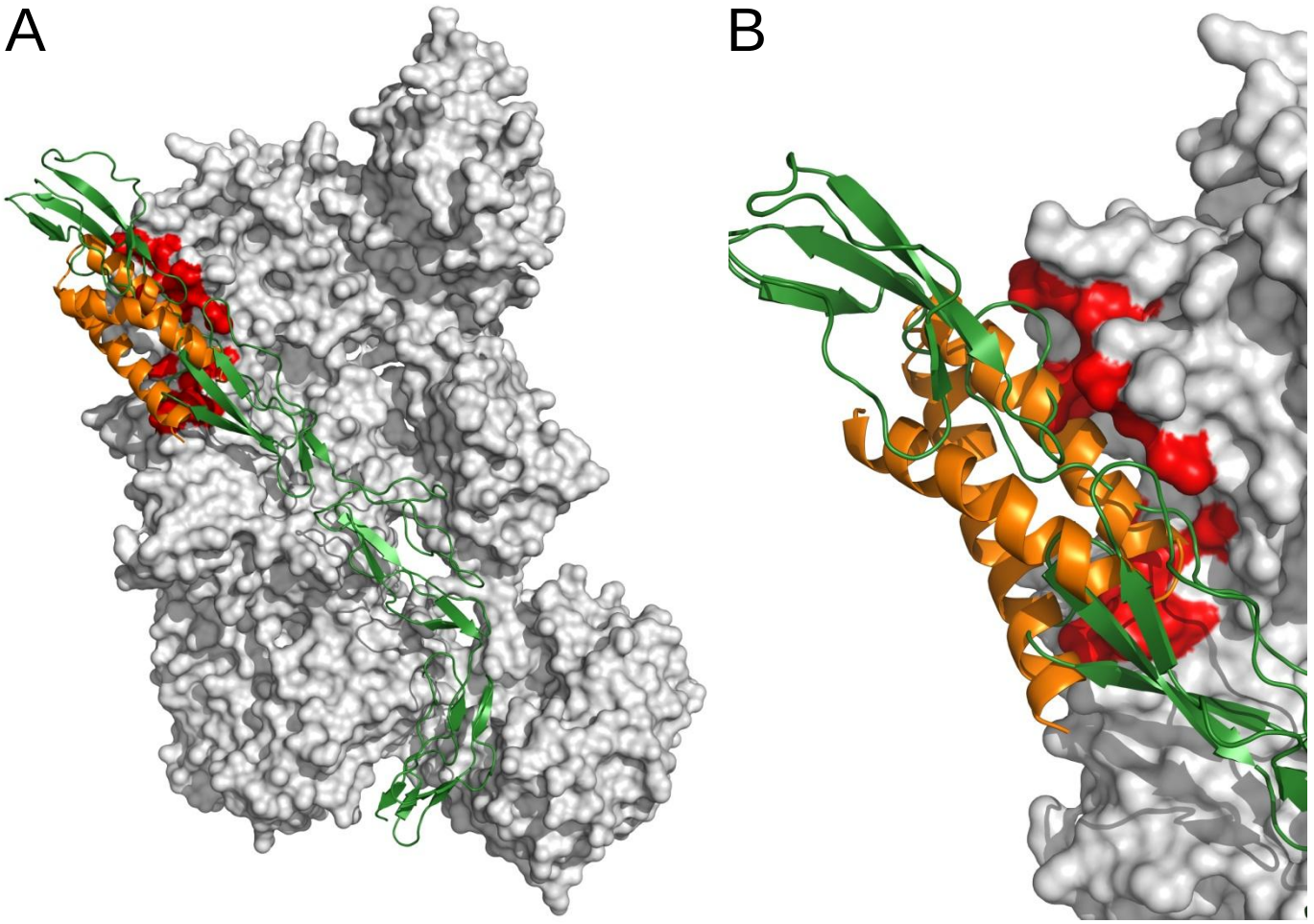

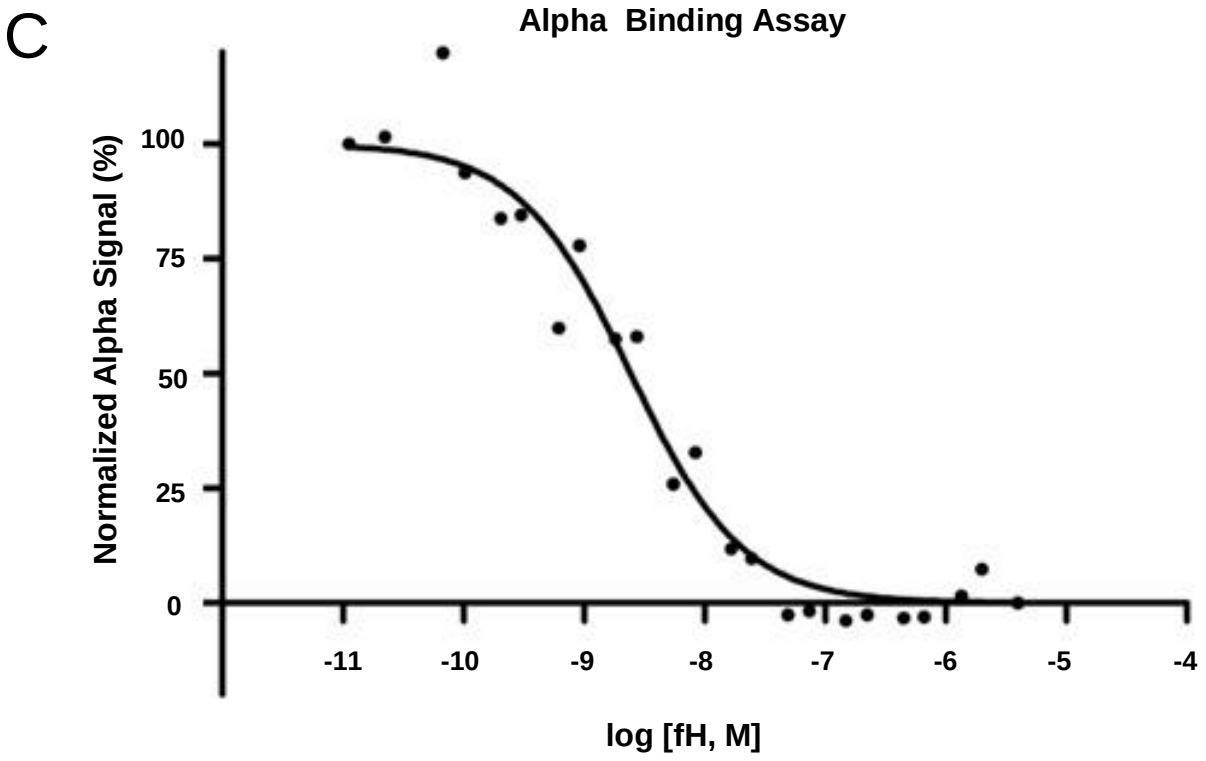

Garcia et al, Fig. S5

A

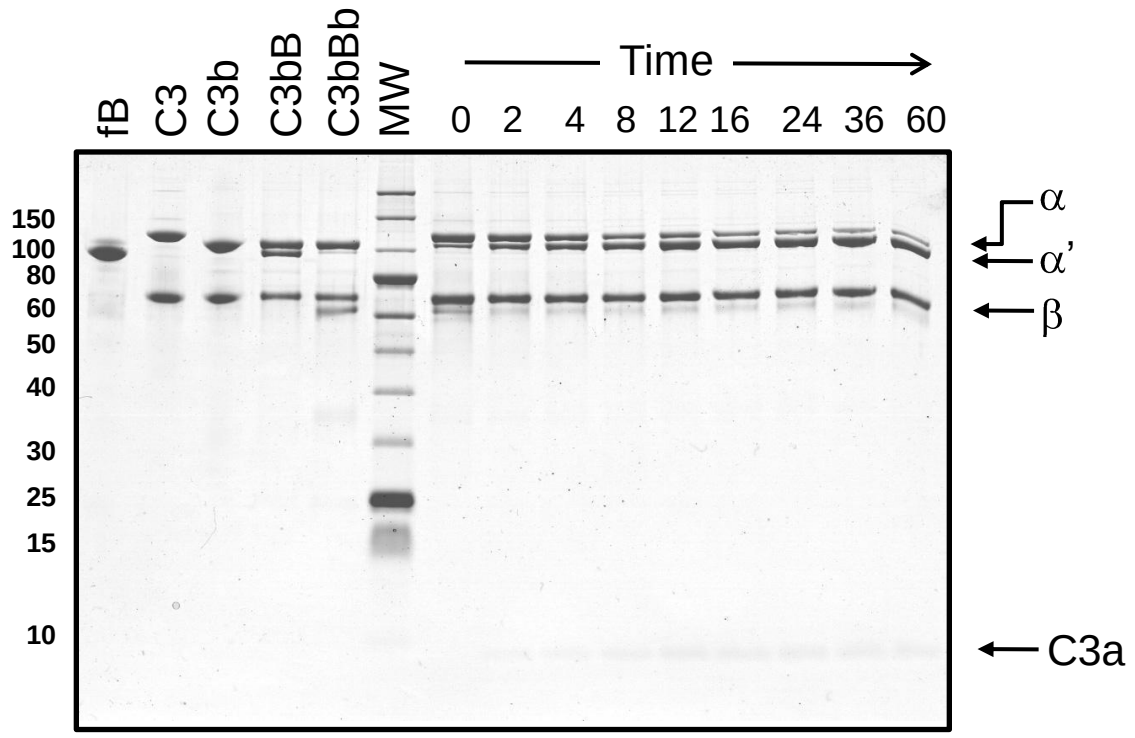

B

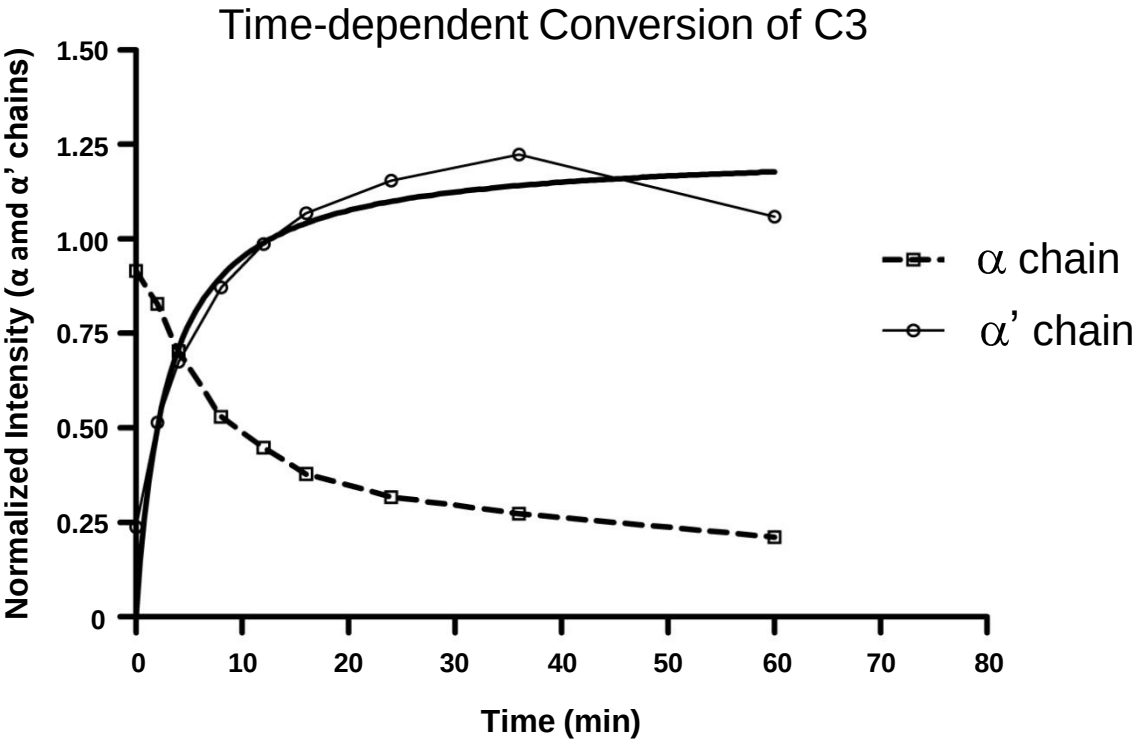

Garcia et al, Fig. S6

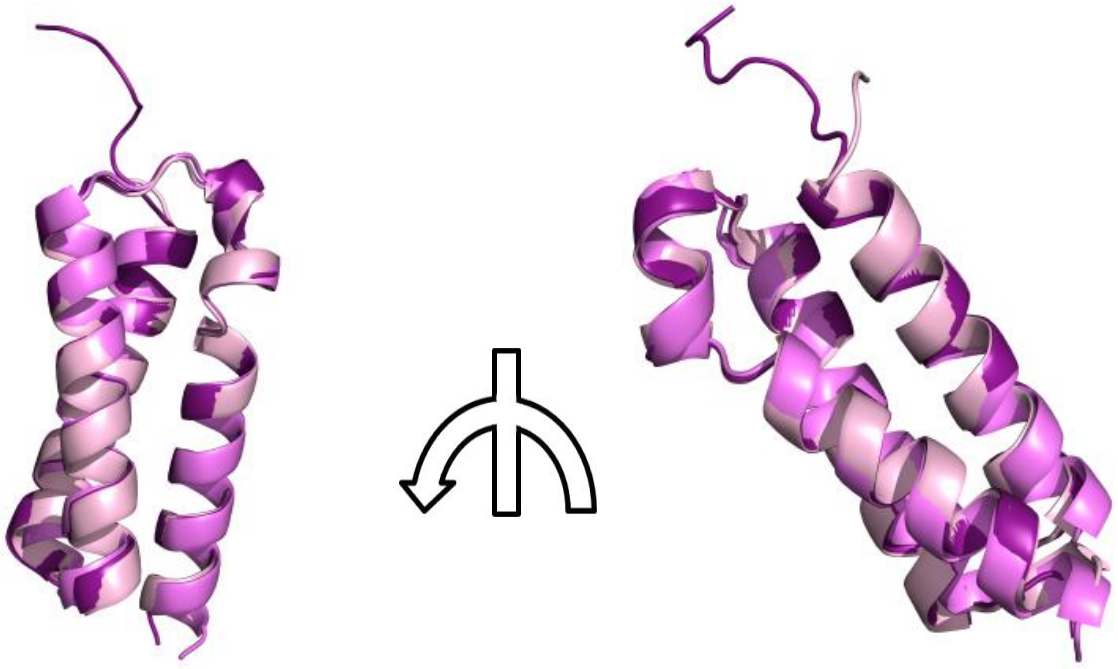

Garcia et al, Fig. S7